From dislocation nucleation to dislocation multiplication in ceramic nanoparticle

Inas Issa[a b,i] , Lucile Joly-Pottuz[a], Jonathan Amodeo[a,c], David J. Dunstan[d], Claude Esnouf[a], Julien Réthoré[b,ii], Vincent Garnier[a], Jérôme Chevalier[a], Karine Masenelli-Varlot[a]

a Univ Lyon, INSA Lyon, UCBL, CNRS, MATEIS, UMR 5510, 69621 Villeurbanne, France

b Univ Lyon, INSA Lyon, CNRS, LAMCOS, UMR 5259, 69621 Villeurbanne, France

c Aix Marseille Univ., Université de Toulon, CNRS, IM2NP,F-13397 Marseille, France

d School of Physics and Astronomy, Queen Mary University of London, London, E1 4NS, UK

Corresponding author details: Tel : +33 (0)47243 7103; e-mail address : **Karine.Masenelli-Varlot@insa-lyon.fr**

ABSTRACT.

Magnesium oxide nanocubes are compressed along the [001] direction *in situ* in the transmission electron microscope. Incipient plasticity in the smaller samples is characterized by the nucleation of few ½<110>{110} dislocations while a larger number of line defects is observed in larger nanocubes. Yield and flow stresses scattered stochastically above a minimum value varying as the inverse of the sample size. The upper bound is given by the reduced number of dislocation sources. Such size-dependent behaviour is justified by a detailed statistical analysis and is fully explained by the deformation mechanism.

---

[i] Now at Department Materials Science, Chair of Materials Physics, Montanuniversität Leoben, Leoben, Austria

[ii] Now at EC Nantes, CNRS UMR6183, GeM, F-44300, France

KEYWORDS. *In situ*, TEM, compression, dislocation, MgO

IMPACT STATEMENT

We unravel the size-dependent strengthening origin in MgO single-crystals using in situ TEM. The proposed lower and upper bound models of the yield stress are applicable to any single-crystalline material.

INTRODUCTION

The strengthening of crystals with decreasing size has been reported in many micromechanical testing configurations and has led to the paradigm of "smaller is stronger" [1]. In single-crystals, compression tests of micropillars and nanoparticles have shown different behaviours as a function of size, crystalline lattice, orientation and surface state [2-5]. A power law fit is generally used to account for the evolution of the yield stress σ_y as a function of the sample size *d* [6]*:*

$$\sigma_y = Ad^{-x} + \sigma_0$$

where *x* and *A* are positive reals, and σ_0 represents the yield stress in bulk single-crystals. The exponent *x* has been reported to range between 0.60 and 0.97 for FCC lattices [7-12], and between 0.22 and 0.48 for BCC crystals [13, 14] with a significant dependence on crystal orientation [15]. Several exponent values have sometimes been found within the same material and, for some sizes, the behaviours of BCC and FCC metals converge [16].

Two main mechanisms have been proposed to account for this size-dependent response. Confinement can lead to line-tension induced strengthening due to the presence of a significant amount of pre-existing dislocations in a limited volume [17-21]. In dislocation-free nano-objects,

plasticity occurs by surface dislocation nucleation events that can alternate with starved states [5, 22-24]. This leads to a stochastic behaviour related to the probability of finding a surface defect on which dislocations can nucleate. Dunstan and Bushby showed that the scaling exponent $x = 1$ was compatible with all available data acquired on pillars, implying that the size effect can be related to the dislocation curvature mechanism in systems originally containing dislocations [25].

We report here a comprehensive experimental study of the size effect and the associated deformation mechanisms in magnesium oxide (MgO) single-crystalline nanocubes. MgO is characterized by dislocation slip in two slip system families, *i.e.* ½<110>{110} and ½<110>{100} [26]. Critical resolved shear stress in MgO exhibit high lattice friction typical of thermally-activated glide processes as shown by the predominance of screw character dislocations, when deformed at room temperature [27, 28, 29]. Herein, we focus on the MgO nanoparticle deformation process, and in particular, on deformation process transition that occurs when changing the sample size, and on its consequence on the stress scaling exponent.

MATERIALS & METHODS

MgO nanocubes were synthesized according to the methods described in supplementary information (SI). The nanocubes are single-crystals and exhibit {100} faces. No bulk lattice defects such as dislocations, grain boundaries or twinning, could be observed in nanocubes smaller than 200-300 nm.

In situ TEM nanocompression tests were carried out using a dedicated specimen holder, see details in SI. Tests were performed with a displacement rate, most often, set to 2 $nm.s^{-1}$. Among all tests performed, only a set of 17 is presented in this study. The selected tests correspond to the most successful ones including best alignment conditions, minimum deviation of the sample

during the test, enhanced contrast and successful post-processing.

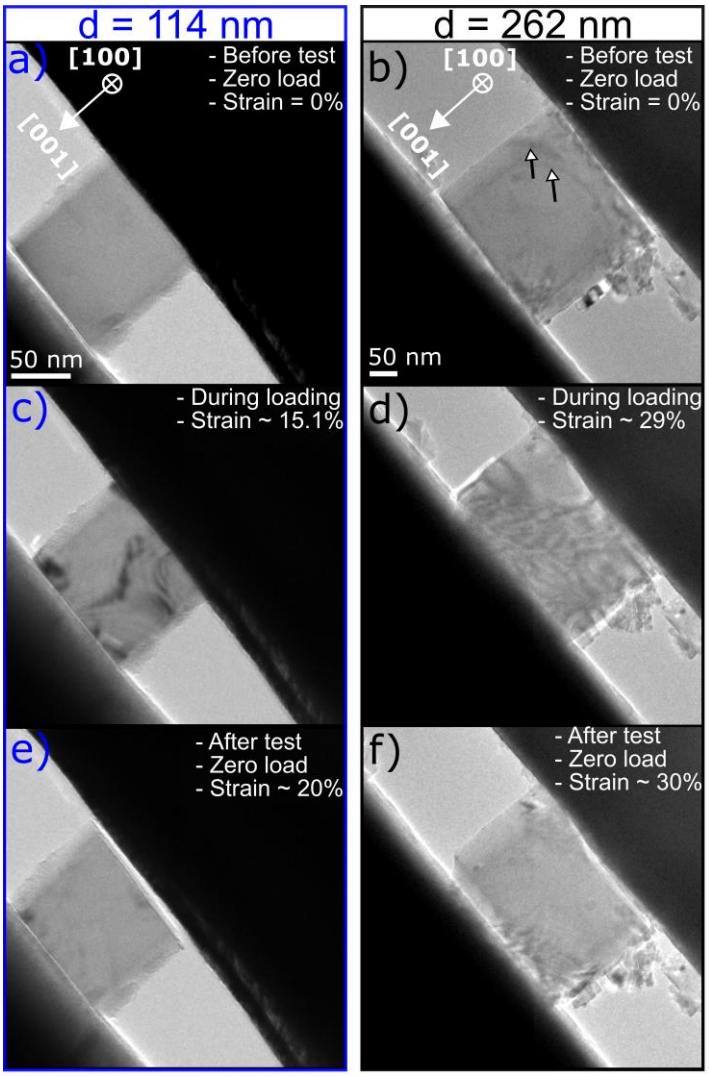

Figure 1. BF TEM images of MgO nanocubes (near [100] zone axis) extracted from compression tests along the [001] direction. a, c, e) nanocube of size 114 nm before load, at ~15.1% and ~20% strain. b, d, f) nanocube of size 262 nm before load, at ~29% and ~30% strain. Two dislocations are indicated by black arrows.

RESULTS

Typical Bright Field (BF) images of a smaller (size 114 nm) and a larger (size 262 nm) MgO

nanocubes, acquired before the compression tests, are provided in Figure 1a and Figure 1b, respectively. Both nanocubes are compressed along the [001] direction and observed along the [100] zone axis. The small nanocube does not show any contrast, which suggests the lack of pre-existing dislocations. This is confirmed by Weak-Beam Dark Field (WBDF) analyses (see SI). On the contrary, the larger nanocube exhibits two thin mobile dark lines attributed to dislocations (see movies available at https://www.youtube.com/channel/UCgqIlZ1X_wbRl1HKsvdFeLw). This confirms that larger nanocubes may contain pre-existing dislocations, whereas the smaller ones are dislocation-free.

In situ TEM compression tests and Molecular Dynamics simulations have shown that the onset of plasticity in dislocation-free MgO nanocubes is governed by nucleation and propagation of ½<110>{110} dislocations [30]. Surface dislocation nucleation and propagation account for the contrasts observed during the test of the 114 nm sized nanocube shown in Figure 1c. After unload (Figure 1e), the smaller sample shows no clear contrasts attributed to a lack of defects (starved state). In the following, the indexation method provided in SI is used to rigorously characterize slip systems and dislocation characters. Figure 2a shows a TEM image of a 195 nm sized nanocube at the onset of plasticity using the WBDF imaging mode, with a zone axis near to the [100] direction and using the diffraction vector **g** = (002). Only a few dislocations appear in the sample, as shown in Figure 2a. Three long screw dislocations segments lying in the $^1/_2[011](01\bar{1})$ slip systems are identified, with short terminations of edge character. We believe that this anisotropic shape is due to the high lattice friction that restricts screw dislocation mobility, as for bulk MgO single crystals deformed at low temperature [29, 30]. In conclusion, the deformation of smaller nanocubes is characterized by consecutive ½<110>{110} surface dislocation nucleation and starvation events that lead to quasi dislocation-free states after unload.

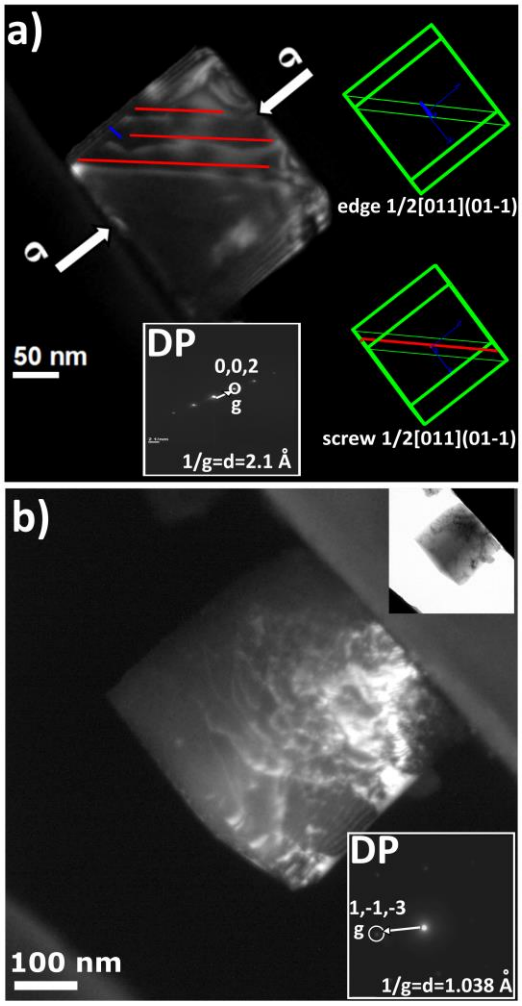

Figure 2. TEM images of nanocubes at different stages of *in situ* compression tests. a) WBDF TEM image using the diffraction vector (002) of a 195 nm nanocube at yield stress. Crystallographic models are shown in the inset. b) WBDF image of a 355 nm sized cube at zero load after 22% true strain (diffraction vector used $\mathbf{g} = [1\bar{1}\bar{3}]$).

Figure 2b shows a dislocation burst originating from a singular contact between the indenter and the top surface. Surprisingly, the sample holds most of the nucleated dislocations after unload. This behaviour is observed in all samples with sizes larger than 200-300 nm that exhibit similar dislocation microstructures. Mechanical responses for larger nanocubes are also smoother than those for smaller ones (Figure 3). Indeed, the larger number of dislocations required to

accommodate plastic deformation (when compared to smaller samples) induces a further discretized and distributed plastic relaxation, thus a better load control when increasing the sample size [21].

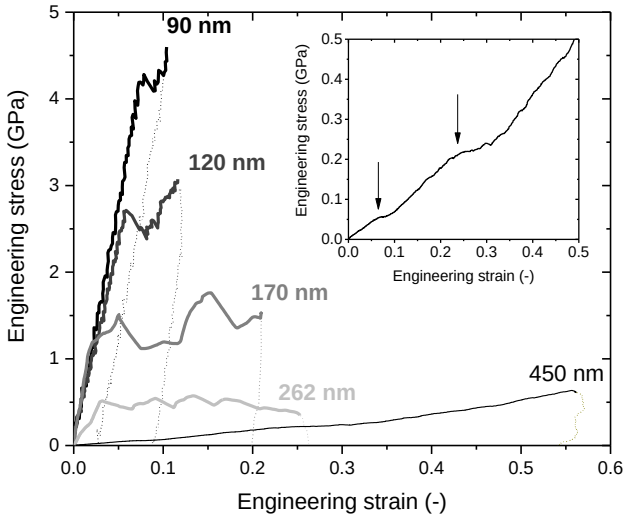

Figure 3. Experimental engineering stress-strain curves of MgO nanocubes of different sizes, all compressed along the [001] direction. The inset shows the onset of the curve for the 450 nm nanocube. Arrows indicate the lower and upper positions of the yield point used to determine the yield stress and its error bar.

Figure 3 shows stress-strain curves for several MgO nanocubes with different sizes, all compressed along the [001] direction. The nanocubes underwent several compression cycles but for clarity reasons, only the first cycles are reported and discussed. The curves obtained for nanocubes with sizes of 90 to 262 nm exhibit well-defined linear regimes (elastic domains). For the smallest nanocubes (90, 120 and 170 nm), the curves have the same slope, equal to that of the unloading part. The 262 nm cube exhibits a slightly lower slope attributed to a slight misalignment of the nanoparticle at the very beginning of the test, which only influences the critical strain (not the nanocube yield strength). For all these cubes, the linear regimes are interspersed by stress drops revealing dislocation nucleation events. The yield stress is then

defined as the maximum stress before the first stress drop.

The curve obtained on the 450 nm cube is far smoother, with no significant stress drop. This behaviour might be justified by a transition in the main deformation process, especially as the initial dislocation content has shown to depend on size. The reduction in the slope of the elastic line is also attributed to nanocube misalignment. We consider that the yield point is thus very uncertain in this specimen and adopt the two break-points marked in the inset of Figure 3 as the upper and lower limits of its error bar.

Yield stresses are shown in figure 4 and corresponding strain rates are summarized in SI. We believe that the observed flow stress variations are related to the size-induced plasticity process transition, i.e. from dislocation nucleation to dislocation multiplication, and to the evolution of dislocation microstructure, i.e. from very few dislocation to numerous dislocation populations, rather than on strain rate (see discussion in SI). Figure 3 emphasizes the size effect where data are fitted with the equations $\sigma = ad^{-x}$ or $\sigma = ad^{-x} + \sigma_0$. A least-squares (LS) fit with a and x as fitting parameters and $\sigma_0 = 0$ returns the exponent $x = 1.1 \pm 0.25$. Fitting σ_0 as well, x drops to 0.7 ± 0.7, with $\sigma_0 = -1 \pm 2$ GPa. Other values of x are also available, e.g. $x = 1.3 \pm 0.2$ when LS fitting of a straight line is done on the log-log axes.

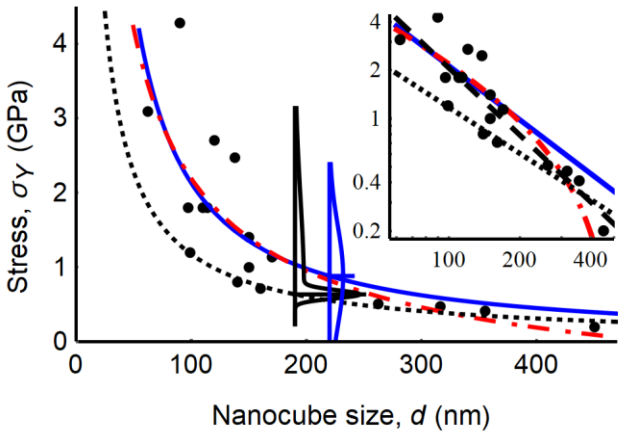

Figure 4. Dependence of the yield stress on the nanocube size. The experimental points (●) are fitted to $\sigma = ad^{-x}$ and $\sigma = ad^{-x} + \sigma_0$ using LS fitting on linear axes (blue lines and chain-dotted red lines, respectively). A LS fitting of a straight line on log-log axes is shown in the inset (dashed black line). The dotted black lines are the result of the outcome of the Maximum Likelihood (ML) fit calculated for $\sigma = ad^{-x}$ with three parameters defining an asymmetric probability distribution functions of the residuals. The two graphs plotted above the 200 nm tickmark show the LS Gaussian pdf (blue) and the ML pdf (black) for the residuals, centred on the respective curves of best fit.

Stress-strain curves obtained on the largest three cubes are quite smooth and reveal continuous plastic flow, typical of dislocation multiplication, whereas the curves obtained on the smallest cubes exhibit well-defined stress drops attributed to nucleation events. Such different trends can be compared with the mild and wild behaviours introduced by Weiss *et al.* [31, 32]. When mild, the scatter of the yield point is expected to be symmetric around the best fit. In contrast, the scatter from the wild data should always lie on or above the best fit, as higher stresses are required to enable dislocation nucleation. So, the expected probability distribution function (pdf) of the residuals should not be the Gaussian assumed by LS fits but a narrower Gaussian with a broader tail on the positive side only. The likelihood of the residuals is calculated for ad^{-x} and maximized with respect to a, x, and three parameters defining the pdf (σ_1 of the narrower Gaussian, σ_2 for the width of the tail, and f for the fraction of the probability that is in the tail). The outcome of this ML fit is $x = 0.95 \pm 0.10$, with $\sigma_1 = 0.06 \pm 0.02$ GPa, $\sigma_2 = 1.3 \pm 0.3$ GPa and $f = 0.66 \pm 0.14$. Comparing this fit with the LS ad^{-x}, the value of the log-likelihood is increased from –17.5 to –10.5. The Bayesian information criterion is decreased from 43.5 to 38.5, which indicates a substantial preference for the ML model. It can be concluded that plasticity in MgO depends on the nanocube size: (i) the lower bound of the yield stress is given by the $1/d$ curve,

and (ii) the nanocubes having a yield stress above this curve exhibit wild plasticity, in agreement with the theory proposed elsewhere [33-35].

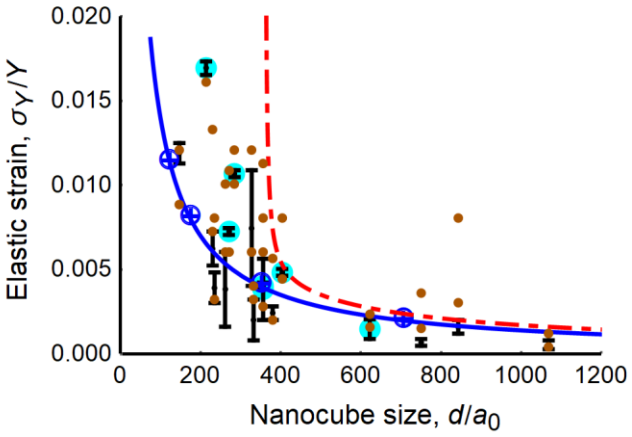

Figure 5. Dependence of the elastic strain (yield stress σ_Y divided by the Young's modulus at bulk Y = 248 GPa) on the normalized nanocube size (linear size d divided by the lattice constant a_0 = 0.421 nm). The brown points are the lowest and highest stresses observed in the range of deformation from 0.2 to 0.3. The cyan highlighting identifies the data where plasticity is governed by dislocation propagation; the other data show the strain bursts and stress drops characteristic of small-scale plasticity (nucleation-starvation mechanism). The blue curve represents the minimum strength that any small volume of material can have when plastic deformation is enabled by normal dislocation multiplication and propagation mechanisms [40]. The red chain-dotted curve is the sum of the size effect equation and the equation of Phani *et al.* [33-35].

DISCUSSION

To investigate the universality of the model, Figure 5 plots MgO nanocubes data in normalized form, *i.e.* stresses divided by Young's modulus (Y = 248 GPa for bulk MgO) and linear sizes divided by the lattice parameter (a_0 = 0.421 nm for MgO). We consider yield points only when they are readily identifiable on the stress-strain curves. In that case, error bars represent

uncertainties on the measured value, due to the signal-to-noise ratio or to the possible presence of a change in slope before the first stress drop. The lowest and highest stresses observed in the range of deformation from 0.2 to 0.3 are also used. We also show data for InGaAs epitaxial strained layers for comparison. InGaAs layers were grown to thicknesses greater than their critical thickness, so that the misfit strain was partially relaxed by plastic deformation [36]. The residual elastic strain for a thickness h was 0.8 nm/h, in good agreement with the prediction from critical thickness theory of ~5b/h where b is the relevant component of the relevant Burgers vector [37]. However, to avoid issues of Schmid factors, this is expressed, rather, as ~1.4a_0/h. The solid blue line, obtained by the fit to the InGaAs data and the above-mentioned theoretical considerations, represents the minimum strength that any small volume of material can have when plastic deformation is enabled by normal dislocation multiplication and propagation mechanisms. The MgO data, within error, are consistent with this size effect, mostly lying close to the minimum strength curve where mild deformation arises ($d/a_0 > 500$) or above the minimum strength curve ($d/a_0 < 500$).

In sufficiently small volumes, especially when the volume is limited by free surfaces, it is possible for the normal dislocation multiplication and propagation mechanisms to be prevented (dislocation starvation). Considering that as the size of a specimen is reduced, the number of dislocation sources or other defects capable of initiating such events may be only a few, Phani *et al.* used Poisson statistics and analysed the results of Monte Carlo simulations [33]. They concluded that an upper bound could be put on the observed scatter of yield strengths between the bulk strength σ_b and the theoretical strength,

$$\sigma_{UB} = \sigma_b \frac{\rho_{1D}\ell}{\rho_{1D}\ell + ln\alpha}$$

where ρ_{1D} is the linear density of such defects (the reciprocal of the average distance between them), ℓ relevant specimen size, and α, taken to be 0.05, the proportion of events that occur above the upper bound. We add this function to the size-effect minimum strength, since it is an additional strengthening mechanism, and plot it in Figure 5, for $1/\rho_{1D}$ = 120 nm and σ_b = 50 MPa, value of the macroscopic yield stress of bulk MgO compressed at room temperature along the <001> direction [29]. Data are then expected to fall anywhere between the minimum strength and this upper bound, as indeed they mostly do. This confirms the stochastic behavior of MgO nanocubes for $d/a_0 < 500$, where nucleation and starvation are the rate-controlling mechanisms. We conclude that the experimental results are explained by and are consistent with the size-effect minimum strength and the number-effect stochastic strengthening. The size dependence is particularly visible in MgO, which combines a very high theoretical strength due to lattice friction and a very low bulk strength. We suggest that such behaviour can be generalized to any monocrystalline nanomaterial – including BCC and FCC metallic single-crystals - but as the size dependence depends on both parameters, its effect may be less pronounced, or the transition may occur at different sizes.

ACKNOWLEDGMENTS

The authors acknowledge the Consortium Lyon Saint-Etienne de Microscopie (CLYM) for the access to the JEOL 2010F microscope.

DECLARATION OF INTEREST STATEMENT

The authors declare no competing interests.

REFERENCES

1. Uchic MD, Dimiduk DM, Florando JN, et al. Sample dimensions influence strength and crystal plasticity. Science 2004;305:986-989.
2. Kiani S, Ratsch C, Minor AM, et al. Orientation- and size-dependent room-temperature plasticity in ZrC crystals. Phil. Mag. 2015;95:985-997.
3. Korte S, Clegg WJ. Discussion of the dependence of the effect of size on the yield stress in hard materials studied by microcompression of MgO. Phil. Mag. 2011;91:1150-1162.
4. Kiener D, Minor AM. Source truncation and exhaustion : insights from quantitative *in situ* TEM tensile testing. Nano Lett. 2011;11:3816-3820.
5. Wagner AJ, Hintsala ED, Kumar P, et al. Mechanisms of plasticity in near-theoretical strength sub-100 nm Si nanocubes. Acta Mater. 2015;100:256-265.
6. Kraft O, Gruber PA, Mönig R, et al. Plasticity in Confined Dimensions. Annual Rev. Mater. Res. 2010;40:293-317.
7. Greer JR, De Hosson JTM. Plasticity in small-sized metallic systems: intrinsic versus extrinsic size effect. Prog. Mater. Sci. 2001;56:654-724.
8. Uchic MD, Shade PA, Dimiduk DM. Plasticity of Micrometer-Scale Single Crystals in Compression. Annual Rev. Mater. Res. 2009;39:361 86.
9. Dou R, Derby B. A universal scaling law for the strength of metal micropillars and nanowires. Scripta Mater. 2009;61:524 27.
10. Jennings AT, Burek MJ, Greer JR. Microstructure versus Size: Mechanical Properties of Electroplated Single Crystalline Cu Nanopillars. Phys. Rev. Lett. 2010;104:135503.
11. Mordehai D, Lee SW, Backes B, et al. Size effect in compression of single-crystal gold microparticles. Acta Mater. 2011;59:5202-15.
12. Sharma A, Hickman J, Gazit N, et al. Nickel particles set a new record of strength. Nature Commun. 2018;9:4102.
13. Kim JY, Jang D, Greer JR. Tensile and compressive behavior of tungsten, molybdenum, tantalum and niobium at the nanoscale. Acta Mater. 2010;58:2355–2363.
14. Schneider AS, Clark BG, Frick CP, et al. Effect of orientation and loading rate on compression behavior of small-scale Mo pillars. Mater. Sci. Eng. A. 2009;508:241–246.
15. Greer JR, Kim JY, Burek MJ. The *in situ* mechanical testing of nanoscale single-crystalline nanopillars. JOM 2009;61:19-25.

16. Huang L, Li QJ, Shan ZW, et al. A new regime for mechanical annealing and strong sample-size strengthening in body centred cubic molybdenum. Nature Commun. 2011;2:547.
17. Bragg L. The strength of metals. Math. Proc. Cambridge Philos. Soc. 1949;45:125-130.
18. Kuhlmann-Wilsdorf D, van der Merwe JH. Theory of dislocation cell sized in deformed metals. Mater. Sci. Eng. 1982;55:79-83.
19. Beanland R. Dislocation multiplication mechanisms in low-misfit strained epitaxial layers. J. Appl. Phys. 1995;77:6217.
20. Dehm G, Balk TJ, von Blanckenhagen B, et al. Dislocation dynamics in sub-micron confinement: recent progress in thin film plasticity. Z. Metallkunde 2002;93:383-391.
21. Dunstan DJ. The size effect in the mechanical strength of semiconductors and metals: strain relaxation by dislocation-mediated plastic deformation. J. Mater. Res. 2017;32:4041-4053.
22. Nix WD, Greer JR, Feng G, et al. Deformation at the nanometer and micrometer length scales: effects of strain gradients and dislocation starvation. Thin solid films 2007;515:3152-3157.
23. Greer JR, Nix WD. Nanoscale gold pillars strengthened through dislocation starvation. Phys. Rev. B 2006;73:245410.
24. Chisholm C, Bei H, Lowry MB, et al. Dislocation starvation and exhaustion hardening in Mo alloy nanofibers. Acta Mater. 2012;60:2258–2264.
25. Dunstan DJ, Bushby AJ. The scaling exponent in the size effect of small scale plastic deformation. Int. J. Plasticity 2013;40:152-162.
26. Amodeo J, Merkel S, Tromas C, et al. Dislocations and plastic deformation in MgO crystals : a review. Crystals 2018;8:240.
27. Amodeo J, Carrez P, Devincre B, et al. Multiscale modelling of MgO plasticity. Acta Mater. 2011;59:2291-302.
28. Appel F, Wielke B. Low temperature deformation of impure MgO single crystals. Mater. Sci. Eng. 1985;73:97-103.
29. Hulse CO, Pask JA. Mechanical properties of magnesia single crystals compression. J. Am. Ceram. Soc. 1960;43:373-378.
30. Issa I, Amodeo J, Réthoré J, et al. In situ investigation of MgO nanocube deformation at room temperature. Acta Mater. 2015;86:295-304.

31. Weiss J, Ben Rhouma W, Richeton T, et al. From mild to wild fluctuations in crystal plasticity. Phys. Rev. Lett. 2015;114:105504.
32. Zhang P, Umut Salman O, Zhang JY, et al. Taming intermittent plasticity at small scales. Acta Mater. 2017;128:351-364.
33. Sudharshan Phani P, Johanns KE, George EP, et al. A simple stochastic model for yielding in specimens with limited number of dislocations. Acta Mater. 2013;61:2489-2499.
34. Morris JR, Bei H, Pharr GM, et al. Size effects and stochastic behavior of nanoindentation pop in. Phys. Rev. Lett. 2011;106:165502.
35. Kwon J, Bowers ML, Brandes MC, et al. Characterization of dislocation structures and deformation mechanisms in as-grown and deformed directionally solidified NiAl-Mo composites. Acta Mater. 2015;89:315-326.
36. Dunstan DJ, Kidd P, Howard LK, et al. Plastic relaxation of InGaAs grown on GaAs. Appl. Phys. Lett. 1991;59:3390-3392.
37. Dunstan DJ. Critical thickness theory applied to micromechanical testing. Adv. Eng. Mater. 2012;14:942-947.